Electrochromic Graphene Molecules

Zhiqiang Ji,[†] Stephen K. Doorn,[‡] and Milan Sykora*,[†]

[†]Chemistry Division, [‡]Materials Physics, Applications Division, Center for Integrated Nano-Technologies, Los Alamos National Laboratory, Los Alamos, New Mexico 87545, United States

ABSTRACT Polyclic aromatic hydrocarbons also called Graphene Molecules (GMs), with chemical composition $C_{132}H_{36}(COOH)_2$ were synthesized *in situ* on the surface of transparent nanocrystalline indium tin oxide (*nc*-ITO) electrodes and their electronic structure was studied electrochemically and spectro-electrochemically. Variations in the potential applied onto the *nc*-ITO/GM electrodes induce only small changes in the observed current, but they produce dramatic changes in the absorption of the GMs, which are associated with their oxidation and reduction. Analysis of the absorption changes using a modified Nernst equation is used to determine standard potentials associated with the individual charge transfer processes. For the GMs prepared here, these were found to be $E_{1,ox}^0 = 0.77 \pm 0.01$ V and $E_{2,ox}^0 = 1.24 \pm 0.02$ V *vs* NHE for the first and second oxidation and $E_{1,red}^0 = -1.50 \pm 0.04$ V for the first reduction. The charge transfer processes are found to be nonideal. The nonideality factors associated with the oxidation and reduction processes are attributed to strong interactions between the GM redox centers. Under the conditions of potential cycling, GMs show rapid (seconds) color change with high contrast and stability. An electrochromic application is demonstrated wherein the GMs are used as the optically active component.

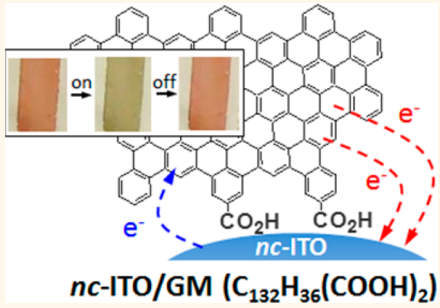

KEYWORDS: graphene molecule · nanographene · graphene · graphene quantum dot · electrochemistry · spectro-electrochemistry · electrochromism

Nanometer-size graphene structures have been recently attracting growing interest because of their potential to play an important role in development of a number of new technologies.[1−4] While expected to retain most of the remarkable electronic, thermal and mechanical properties of bulk graphene, unlike graphene, nanographenes are predicted to have a nonzero band gap tunable by variation of their size.[5−7] Understanding of how to tune the absorption and emission of nanographenes from near-infrared to visible wavelengths and how to control charge-injection into nanographenes and its effect on their properties could open a path for their exploitation in optoelectronic applications, such as photovoltaics, optical detectors, displays, sensors, *etc*. This understanding has so far been limited. This is in part due to the difficulties with preparation of well-defined structures and in part due to limited experimental studies of electronic structure of nanographenes.

Nanographene structures called graphene molecules (GMs) are polycyclic aromatic hydrocarbons (PAHs) typically comprising fewer than 300 carbon atoms, with size of less than five nanometers. Recently developed methods for a "bottom-up" synthesis of GMs[8−10] and their solubilization[2,11,12] facilitated experimental studies of their optical properties[13,14] and revealed absorption tunability through visible and near-infrared wavelengths. The studies of charging of GMs by electrochemical methods, while attempted,[13] were not yet successful. Here we use a recently developed synthetic method[15] to prepare GMs directly on the surface of nanocrystalline indium−tin oxide (*nc*-ITO) electrodes and show that these surface synthesized GMs can be effectively charged, with a high level of control, by an electrochemical potential applied onto the electrode. We demonstrate that optical monitoring of the *nc*-ITO/GM film during charging yields quantitative information about: (1) the absolute energies required for GM charge injection and the electronic structure of GMs, (2) effect of charging on the absorption properties of the GMs, and (3) the kinetics of the *nc*-ITO/GM interfacial charge transfer. Finally, we demonstrate how the basic understanding of the nanographene charging processes can be effectively exploited in a practical application, such as electrochromic devices, wherein a "bottom-up" synthesized

* Address correspondence to sykoram@lanl.gov.

Received for review January 6, 2015 and accepted March 13, 2015.

Published online March 13, 2015
10.1021/acsnano.5b00093

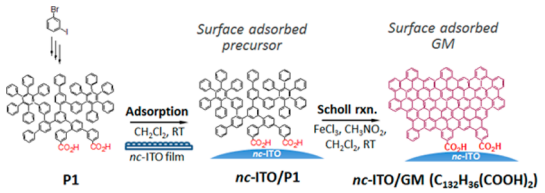

Scheme 1. Abbreviated summary of the procedure for the preparation of *nc*-ITO/GM electrode.

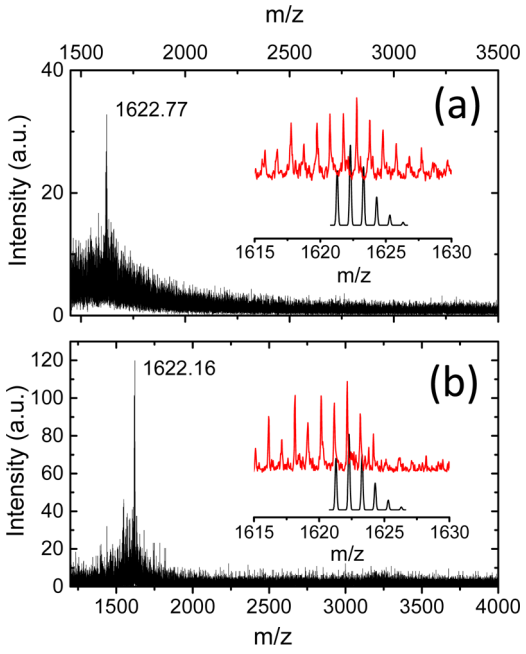

Figure 1. MALDI-TOF mass spectra of (a) GMs synthesized on *nc*-ITO surface, after desorption from *nc*-ITO surface by a dilute HF/HCl and (b) the same GMs independently synthesized in solution.[15] The molecular weight of the highest intensity mass peak is indicated. The laser energy used in the experiment was 13 μJ. Insets: the experimental (red curves) and calculated (black) isotope distribution for mass peak of $C_{132}H_{37}^+$.

nanographene structure with an inherent bandgap is used as the optically active component.

RESULTS AND DISCUSSION

An abbreviated summary of the *nc*-ITO/GM preparation procedure is shown in Scheme 1 (for more details see Methods section). In a typical experiment, a solution of presynthesized precursor P1 was chemisorbed, *via* a carboxylic acid group, onto the porous *nc*-ITO surface. The adsorbed P1 was subsequently oxidized, *in situ*, to form surface adsorbed GMs. In the present work we synthesized and studied GMs with the chemical composition $C_{132}H_{36}(COOH)_2$. The composition and purity of the GMs was verified by MALDI mass-spectroscopy, whereby the GMs were first desorbed from the *nc*-ITO. The mass spectra (MS) of the surface synthesized GMs and the GMs synthesized independently in solution are shown in Figures 1, panels a and b, respectively. Both MS are dominated by a major peak at 1622 *m/z* units, consistent with the formation of $C_{132}H_{36}(COOH)_2$. An absence of major peaks at *m/z* >

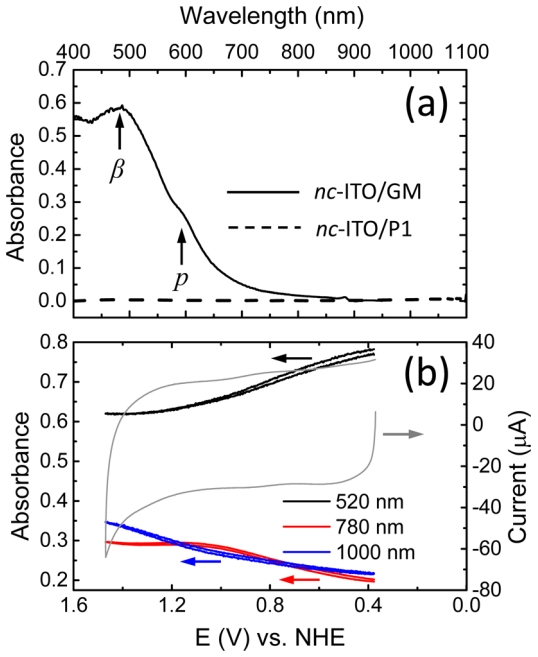

Figure 2. (a) Absorption spectra of the solid, dry *nc*-ITO/GM film (solid trace) and *nc*-ITO/P1 film (dashed trace). The spectra were obtained by subtracting the absorption of the blank *nc*-ITO film. Two distinct features, an absorption peak at ~490 nm (2.57 eV) and a shoulder at ~590 nm (2.12 eV), are assigned to the β (S0 → S2) and *p* (S0 → S1) transitions, respectively, based on previous analysis of the electronic absorption spectra of polyclic aromatic hydrocarbons by Clar *et al.*[33] (b) Cyclic voltammogram of *nc*-ITO/GM film (gray trace) and the variations in the absorption spectrum of the film observed during the CV measurement, monitored at 520 nm (black trace), 780 nm (red trace), and 1000 nm (blue trace). The measurements were performed at room temperature in propylene carbonate with 0.5 M LiTFSI as supporting electrolyte, with scan rate of 5 mV/s.

1622 indicates the completion of the dehydrogenation reaction and lack of significant contamination.

Figure 2a shows typical absorption spectra of the *nc*-ITO/P1 and *nc*-ITO/GM films. The appearance of a broad visible absorption band for the latter is consistent with the formation of a large conjugated aromatic system. Figure 2b shows a typical cyclic voltammogram (CV) of a *nc*-ITO/GM film. In the region of ~0.4−1.5 V, a large capacitive current (attributed to a large surface area of the *nc*-ITO) was observed, with no distinctive peaks indicative of GM charging, regardless of the scan rate. However, the variations in the applied potential induced significant changes in the *nc*-ITO/GM film absorption that can be related to the injection of charges into the GMs. The film absorption variations observed at several wavelengths are shown in black, blue and red colors in Figure 2b. Besides the variations in the magnitude of the induced absorption changes with the wavelength, we also detected two distinct types of dependency on the potential. For example, as shown in Figure 2b, in the spectral region around 780 nm the absorption increases between ~0.4 and ~1.1 V reaching a plateau at ~1.4 V. In contrast, the

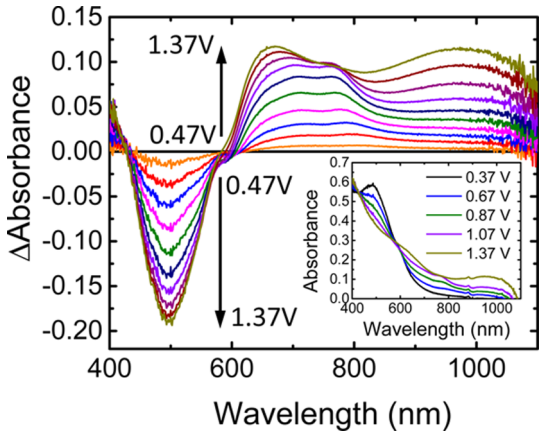

Figure 3. Difference absorption spectra of *nc*-ITO/GM film as a function of the applied potential. The spectra were generated by subtraction of the spectrum obtained at 0.37 V from spectra at the indicated potential (all potential step increments are 0.1 V). The inset shows the absolute spectra of the same film at indicated potentials. All potentials are reported *vs* NHE.

absorption at around 1000 nm shows a monotonic increase to ~1.4 V *vs* NHE. This observation suggests the presence of two distinct charge transfer processes.

Figure 3 shows a summary of the changes in the absorption spectrum of the *nc*-ITO/GM film observed following a series of potential steps. In the spectral range ~420−600 nm, a step to a potential ≥0.47 V produces a distinct bleach with the maximum at ~500 nm. In the spectral region 600−1100 nm, several broad new bands are observed. To better understand the nature of these optical changes and to gain a more quantitative insight into the thermodynamics of the underlying charge transfer processes, the data in Figure 3 were globally fit by a modified Nernst equation in the form of eq 1:

$$\begin{aligned}\Delta A(\lambda) &= \Delta A_1(\lambda) + \Delta A_2(\lambda) \\ &= a_1(\lambda)[\beta_1/(\beta_1+1)] + a_2(\lambda)[\beta_2/(\beta_2+1)] \quad (1)\end{aligned}$$

where

$$\beta_1 = \exp[\alpha_1(E - E_1^0)/k_BT]$$

and

$$\beta_2 = \exp[\alpha_2(E - E_2^0)/k_BT]$$

In eq 1, ΔA is a differential absorbance, E is the applied potential, k_B is the Boltzmann constant, and T is temperature. The adjustable parameters a_1 and a_2, E_1^0 and E_2^0, and α_1 and α_2 are, respectively, the scaling constants, the standard redox potentials, and the nonideality factors associated with the redox processes "1", and "2". Two different processes were assumed to contribute to the observed absorption changes based on the CV results discussed above. The nonideality factor is discussed in more detail in following sections. The results of the global fitting are graphically summarized in Figure 4.

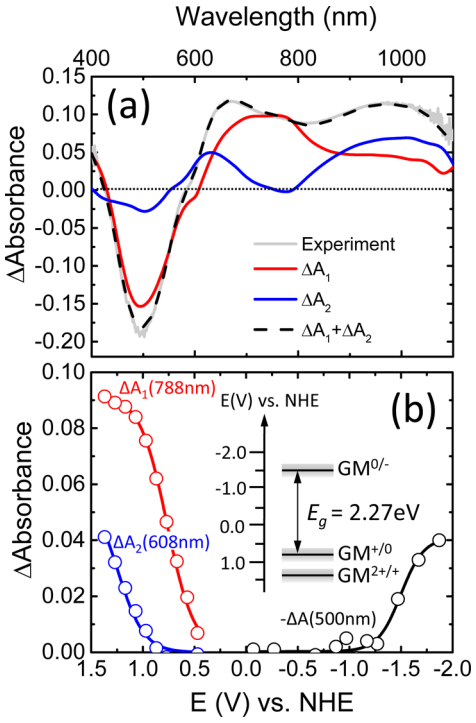

Figure 4. (a) Experimental difference absorption spectra of *nc*-ITO/GM film (gray trace) and the best global fit of eq 1 to the experimental data (black dashed trace) for E = 1.37 V. The spectra of two components, ΔA_1 (red trace) and ΔA_2 (blue trace) comprising the best global fit for E = 1.37 V. (b) Variation of the absorbance with applied potential at 608 nm (blue), 788 nm (red). The symbols are the experimental data and the solid lines are the best global fits of eq 1 to the data shown in Figure 3. The black symbols show experimentally observed variation in the film absorbance at 500 nm at negative potentials. The solid line is the best fit to a one term modified Nernst equation. See Supporting Information for more details. For clarity, the data are shown as −ΔAbsorbance.

Figure 4a shows a comparison of the experimental spectrum (gray trace) and the spectrum of the best global fit to eq 1 (black dashed trace) at the potential of 1.37 V. A similar quality of fit was observed for data at all other potentials. This fit to the experimental data yields two distinct standard potentials E_1^0 and E_2^0, attributed to the processes shown in eqs 2 and 3 below:

$$GM - e^- \rightarrow GM^{+\bullet} \qquad E_{1,ox}^0 = 0.77 \pm 0.01\,V \quad (2)$$

$$GM^{+\bullet} - e^- \rightarrow GM^{2+} \qquad E_{2,ox}^0 = 1.24 \pm 0.02\,V \quad (3)$$

Broad features with very similar peak potential values were observed in differential pulse voltammetry and square wave voltammetry measurements (see Supporting Information). The value of the first oxidation potential, $E_{1,ox}^0$, determined here is very similar to the value of the ionization potential (IP = 0.8 V *vs* NHE) obtained previously for a similar structure by UV photoelectron yield spectroscopy.[13] Using the best fit parameters, we can calculate the spectra ΔA_1 (=$A(GM^{+\bullet})$ − $A(GM)$) and ΔA_2 (=$A(GM^{2+})$ − $A(GM^{+\bullet})$).

These are shown as blue and red traces in Figure 4a, respectively. To the best of our knowledge, these data represent the first report of the absorption spectra of the oxidized GMs. The observation of the strong $GM^{+\bullet}$ absorption in the 700−800 nm region is consistent with previous observations of red shifts of the main absorption band upon chemical oxidation in smaller polycyclic aromatic hydrocarbons.[16] An empirical relationship proposed by Khan *et al.*,[17] $E_A = 0.32 + 0.60E_p$, between the energy of the *p*-band in the absorption spectrum of the neutral PAHs (E_p) and the lowest-energy transition of their radical cation (E_A) can be used to estimate that for the GM studied here the lowest-energy electronic transition in $GM^{+\bullet}$ should be observed at ∼780 nm. This is in good agreement with the results shown in Figure 4a. Our observation of GM^{2+} is consistent with previous theoretical predictions[18] and experimental observations of doubly oxidized PAHs.[19] We note that in a recent study[20] it was reported that graphene, when positively charged, can under ambient conditions spontaneously form graphene oxide, with the reaction rate depending on the graphene oxygen coverage. This process is unlikely to be significantly contributing to our observations. In addition to the evidence supporting the reversible formation of $GM^{+\bullet}$ summarized above, we find that the observed kinetics, as well as the spectral changes, are identical in the experiments performed in air and in strictly anaerobic conditions (see Supporting Information).

A notable feature of the absorption spectra ΔA_1 and ΔA_2 is the presence of isosbestic points at 608 nm in spectrum A_1 and at 550, 760, and 788 nm in spectrum A_2. Since at the isosbestic point the absorption spectrum of only one of the oxidized species changes with the applied potential, these points can be used to independently monitor the $GM^{+\bullet}$ and GM^{2+} formation. The absorption changes observed at 788 nm ($GM^{+\bullet}$ formation) and 608 nm (GM^{2+} formation), and the curves generated by the parameters obtained from the best global fit of eq 1 to the data in Figure 3, are shown in Figure 4b. The curves clearly show distinct onsets for the two oxidations, consistent with the different oxidation potentials of the processes (2) and (3). Also shown in Figure 4b are the changes in the absorption of the *nc*-ITO/GM film observed at negative potentials, measured in a separate experiment (see section 2 in Supporting Information). In this case, no induced absorption was observed in the monitored spectral range. However, similar to positive potentials, we observed the bleaching of the main absorption band at ∼500 nm and attributed it to GM one electron reduction as shown in eq 4:

$$GM + e^- \rightarrow GM^- \qquad E_{1,red}{}^0 = -1.50 \pm 0.04\,V \quad (4)$$

Using these results, we calculate the electrochemical HOMO−LUMO energy gap of the GMs studied here to

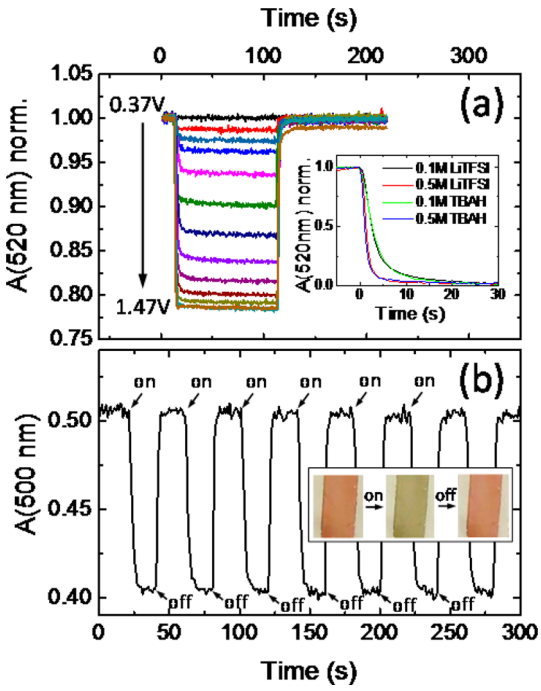

Figure 5. (a) Absorption of *nc*-ITO/GM film at 520 nm as a function of time at indicated potentials (all potential step increments are 0.1 V). The inset shows the variation in the absorption changes as a function of concentration and type of electrolyte. All potentials are *vs* NHE. For experimental details see text. (b) Electrochromic properties of GMs. Main panel: Variation of the *nc*-ITO/GM electrode absorbance at 500 nm upon potential cycling between 0.37 and 1.27 V. The arrows labeled "on" and "off" indicate where the potential is set to 1.27 V and reset to 0.37 V, respectively. The experiment was performed in propylene carbonate, 0.5 M in LiTFSI. Inset: Photographs of *nc*-ITO/GMs film following a potential step from 0.37 to 1.27 V (on) and from 1.27 to 0.37 V (off).

be $E_g = (E_{1,ox}{}^0 - E_{1,red}{}^0) = 2.27 \pm 0.05$ eV. This is consistent with the energy gap of similar structures obtained previously by UV photoelectron spectroscopy[13] and is similar to the energy of the lowest energy p-transition in the absorption spectra of the GMs at 2.12 eV. On the basis of the above analysis, the spectral changes observed during the oxidation (Figure 3) or reduction of the GMs are associated with the depopulation of their HOMO or population of the LUMO frontier orbitals, respectively. This is similar to the mechanism used to explain the bleaching of the optical transitions of bulk graphene induced by an applied bias.[21] Because charging leads to a significant distortion of the electronic structure of the small-size GMs, the bleaching of the HOMO−LUMO ("band edge") transition in the neutral GMs at ∼500 nm is accompanied by the appearance of new induced absorption features associated with the formation of charged GMs.

The nonideality factor, α, in eqs 1 and (S1 of Supporting Informaton) is introduced to account for the nonideal Nernstian behavior of the experimental system. The best fits yielded values of $\alpha_1 = 0.19 \pm 0.01$ and

$\alpha_2 = 0.20 \pm 0.03$ for oxidations and a value $\alpha = 0.23 \pm 0.06$ for the reduction, distinctly different from the ideal behavior ($\alpha = 1$). The non-Nernstian behavior of surface adsorbed redox species was observed previously and several explanations were proposed.[22−24] Here we attribute the observed non-Nernstian behavior to strong electronic interactions between the individual GMs (see Methods section for more details).

Figure 5a shows temporal changes in the absorption of the *nc*-ITO/GM film observed at various applied potentials. The observed changes in the optical absorption are rapid (seconds) and highly reversible up to the potential of ~1.5 V. The inset shows that the GM oxidation rate is independent of the supporting electrolyte type, but is dependent on its concentration. The observation of rapid, reversible changes of the absorption properties of the *nc*-ITO/GM films with applied potential prompted us to study their electrochromic properties.

New electrochromic materials are of great interest for application in displays and smart windows.[25,26] For the material to have a potential to be used in these practical applications it should have high coloration efficiency (change in optical density per unit inserted charge), high contrast between "on" and "off" states, fast switching response, large cycle life, spectral tunability and low cost. The potential of graphene in electrochromics was demonstrated previously. Flexible electrochromic devices based on electro-modulation of multilayer bulk graphene were shown to provide optical modulation up to 55% in visible and near-infrared spectral ranges.[27] Reversible electrochromic behavior, as well as tunable ultrafast optical response, under applied bias was also reported for multilayer graphene oxide thin films.[20,28] Here we study, for the first time, the electrochromic properties of "bottom-up" synthesized graphene nanostructures with size-tunable electronic band gap.

Figure 5b shows the reversible color changes observed for the *nc*-ITO/GM films upon potential cycling between 0.37 and 1.27 V *vs* NHE. Under the indicated conditions, we found the coloration efficiency of the *nc*-ITO/GM films to be 60−110 cm^2/C, maximum contrast of 32% and switching rate of less than 4 s. The electrochromic changes were persistent for more than five thousand cycles. These performance characteristics of our first generation devices are comparable with the state-of-the-art electrochromic inorganic materials[29] and conductive polymers.[30] The results represent an encouraging step toward exploitation of GMs and their size dependent electronic properties in electrochromic devices.

CONCLUSIONS

We synthesized GMs with composition $C_{132}H_{36}(COOH)_2$ on the surface of *nc*-ITO electrode and studied their electronic and charge transfer properties by electrochemical and spectroelectrochemical methods. We showed that one and two electron oxidations and one electron reduction of GMs can be observed within the electrode potential window. By analyzing the data with the modified Nernst expression, we were able to determine the standard oxidation and reduction potentials of the GMs and their electrochemical HOMO−LUMO gap. Finally, we demonstrated that GMs are promising materials for electrochromic applications.

METHODS

Preparation of *nc*-ITO. The *nc*-ITO films were prepared by a modified literature procedure.[31] ITO nanopowder (particle size ~10−20 nm) from Inframat Advanced Materials (3.1 g), acetic acid (3 g), and ethanol (10 mL) were mixed in a 22 mL vial. The mixture was sonicated for 20 min in a bath sonicator. Polyethylene glycol (MW 20 000, 1 g) was added, and the mixture was stirred overnight. The *nc*-ITO films were prepared by doctor-blading method where one layer of Scotch tape was used to mask the surface of FTO glass slide prior to *nc*-ITO paste deposition. To achieve high conductivity, the deposited films were annealed in two steps. First, the films were heated in air at 500 °C for 1 h (ramp: 5 °C/min), and then at 300 °C for 1 h. (ramp: 5 °C/min) under a mixture of 6% H_2/94% N_2. The procedure yields films light blue in color, with thickness of ~3 μm. The films were stored under ambient conditions before use.

Preparation of *nc*-ITO/GM. The precursor P1 was prepared by solution chemistry as described previously.[15] To adsorb precursor P1 onto the films, the *nc*-ITO films were soaked in a dichloromethane solution of P1 (~0.1 mM) overnight. The films were washed with CH_2Cl_2, and then treated with $FeCl_3$ (10 mg/mL) in CH_3NO_2/CH_2Cl_2 (1/3, v/v) for 1 h under argon (Scholl reaction conditions). A dramatic change in color of the *nc*-ITO film can be observed by naked eye during the treatment, indicating formation of a conjugated structure consistent with GM formation. The *nc*-ITO/GM films were then washed with MeOH to remove excess $FeCl_3$.

Mass Spectroscopy of *nc*-ITO Surface Adsorbed GMs. For the MALDI Mass-Spectroscopy studies the GMs were desorbed from the surface of the *nc*-ITO. To achieve that, the *nc*-ITO/GM particles were exposed to a mixture of HF/HCl (0.5 M each) for 3−4 days. The desorbed GMs were collected by centrifugation, washed extensively with DI water and air-dried. Subsequently, the dried GMs were solid-mixed with the TCNQ (tetracyanoquinodimethane) matrix for MALDI analysis. In all studied samples, the mass spectra were dominated by a peak at 1622 *m*/*z* units, attributed to the fully conjugated structure with the composition $C_{132}H_{36}(COOH)_2$, less the carboxylic acid functional groups (chemical formula $C_{132}H_{37}^+$). The decarboxylation of the GMs and slight deviation of the experimental and calculated patterns observed in some cases are attributed to the effects of high laser power required for the ionization of the samples.

Electrochemistry and Spectro-Electrochemistry Experiments. Cyclic voltammograms were recorded using a CH Instruments electrochemical workstation. Typically, all electrochemistry, spectroelectrochemistry, and electrochromism experiments were performed in a 3-electrode setup with *nc*-ITO/GM as a working electrode, Ag wire as a pseudo reference electrode, Pt wire as a counter electrode in separated compartments and propylene carbonate (PC) as a solvent. Various electrolytes including *n*-tetrabutylammonium hexafluorophosphate (TBAH) and lithium bis(trifluoromethane sulphone)imide (LiTFS) in dry propylene carbonate (PC) were used as an electrolyte. The Ag reference electrode was calibrated with Fc^+/Fc redox couple.

The changes in the optical properties of the working electrode upon application of a potential were monitored with an Agilent 8453 UV−vis diode array absorption spectrometer. The reductive side electrochemical and spectro-electrochemical measurements were performed in a glovebox under Argon atmosphere. The absorption changes were monitored using a fiber optic Ocean Optics UV−vis 2000+ absorption spectrometer.

Analysis of the Physical Origin of the Nonideality Factor. To better understand the origin of the nonideal behavior in the case of *nc*-ITO/GM films studied here, we first verified that it is not a property of the electrode. For that purpose, electrodes modified with Ru(bpy)(bpy-PO_3H_2)$_2Cl_2$ complex were prepared and their spectro-electrochemical response was studied using the Nernst-type analysis similar to the one described in main text (see Supporting Information, Figures S5 and S6). For the Ru complex modified electrodes, we find that the data can be well fit with a single term standard Nernst equation (*i.e.*, $\alpha = 1$), which indicates that in the case of *nc*-ITO/GM films the nonideal behavior is an inherent property of the GMs. On the basis of the results of our MS studies as well as the observation of a distinct isosbestic point in the spectro-electrochemical data, we conclude that there is no significant variation in the electronic properties of the GMs; *i.e.*, that the GMs form a uniform ensemble in terms of their electronic structure. To determine if the non-Nernstian behavior may be caused by the potential drop at the electrode surface, spectro-electrochemical experiments were performed using two different supporting electrolytes, LiTFSI and *n*-tetrabutylammonium hexafluorophosphate (*n*TBAH). Since we detected no difference in the redox behavior of the films in these two electrolytes, consistent with previous studies,[24] we infer that non-Nernstian behavior of the GMs is not related to the potential drop effect. Therefore, the non-Nernstian behavior observed for the *nc*-ITO/GM films is attributed to the Frumkin-type behavior, which has been frequently observed for surface attached redox couples, conducting polymers, and inorganic quantum dot films. In this model, the nonideality factor α is related to the interaction energy of the charged species by the expression $\alpha = 1/(1 - \sigma/2)$,[32] where σ is the interaction parameter equal to W/RT, where W is the interaction energy, R is the gas constant and T is temperature. For $\alpha \sim 0.2$ observed for all the charge transfer processes, we can calculate the interaction energy to be $W = -0.21$ eV. The negative sign indicates repulsive interaction. This analysis indicates that the intermolecular interactions significantly impact the oxidation and reduction potentials of individual GMs. Interestingly; the presence of an isosbestic point at 608 nm in the spectroelectrochemistry data (Figure 3) suggests that these electronic interactions do not significantly affect the optical properties of the neutral GMs. In other words, any interaction-induced energy shifts seem to affect the filled and vacant molecular orbitals equally. This observation is similar to the results of previous theoretical studies,[7] which indicate that the peripheral functionalization of GMs with electron withdrawing or donating groups affects the absolute energies of the frontier orbitals, but not the size of the HOMO−LUMO gap.

Conflict of Interest: The authors declare no competing financial interest.

Supporting Information Available: Spectroelectrochemical characterization of *nc*-ITO, *nc*-ITO/Ru-complex and *nc*-ITO/GMs films. This material is available free of charge *via* the Internet at http://pubs.acs.org.

Acknowledgment. Z.J., S.K.D, and M.S. acknowledge the financial support by the Los Alamos National Laboratory Directed Research and Development (LDRD) program. This work was performed in part at the Center for Integrated Nanotechnologies, a U.S. Department of Energy, Office of Basic Energy Sciences user facility. We thank Dr. Cortney Kreller for the assistance with *nc*-ITO film preparation.

REFERENCES AND NOTES

1. Zhi, L.; Müllen, K.; Bottom-up, A. Approach from Molecular Nanographenes to Unconventional Carbon Materials. *J. Mater. Chem.* **2008**, *18*, 1472–1484.
2. Yan, X.; Li, B.; Li, L.-s. Colloidal Graphene Quantum Dots with Well-Defined Structures. *Acc. Chem. Res.* **2012**, *46*, 2254–2262.
3. Bacon, M.; Bradley, S. J.; Nann, T. Graphene Quantum Dots. *Part. Part. Syst. Charact.* **2013**, *31*, 415–428.
4. Li, L.; Wu, G.; Yang, G.; Peng, J.; Zhao, J.; Zhu, J.-J. Focusing on Luminescent Graphene Quantum Dots: Current Status and Future Perspectives. *Nanoscale* **2013**, *5*, 4015–4039.
5. Son, Y. W.; Cohen, M. L.; Louie, S. G. Energy Gaps in Graphene Nanoribbons. *Phys. Rev. Lett.* **2006**, *97*, 216803.
6. Ritter, K. A.; Lyding, J. W. The Influence of Edge Structure on the Electronic Properties of Graphene Quantum Dots and Nanoribbons. *Nat. Mater.* **2009**, *8*, 235–242.
7. Mandal, B.; Sarkar, S.; Sarkar, P. Exploring the Electronic Structure of Graphene Quantum Dots. *J. Nanopart. Res.* **2012**, *14*, 1–8.
8. Muellen, K. Evolution of Graphene Molecules: Structural and Functional Complexity as Driving Forces behind Nanoscience. *ACS Nano* **2014**, *8*, 6531–6541.
9. Feng, X.; Pisula, W.; Müllen, K. Large Polycyclic Aromatic Hydrocarbons: Synthesis and Discotic Organization. *Pure Appl. Chem.* **2009**, *81*, 2203–2224.
10. Chen, L.; Hernandez, Y.; Feng, X.; Müllen, K. From Nanographene and Graphene Nanoribbons to Graphene Sheets: Chemical Synthesis. *Angew. Chem., Int. Ed.* **2012**, *51*, 7640–7654.
11. Yan, X.; Cui, X.; Li, L.-s. Synthesis of Large, Stable Colloidal Graphene Quantum Dots with Tunable Size. *J. Am. Chem. Soc.* **2010**, *132*, 5944–5945.
12. Narita, A.; Feng, X.; Hernandez, Y.; Jensen, S. A.; Bonn, M.; Yang, H.; Verzhbitskiy, I. A.; Casiraghi, C.; Hansen, M. R.; Koch, A. H. R.; et al. Synthesis of Structurally Well-Defined and Liquid-Phase-Processable Graphene Nanoribbons. *Nat. Chem.* **2014**, *6*, 126–132.
13. Yan, X.; Li, B.; Cui, X.; Wei, Q.; Tajima, K.; Li, L.-s. Independent Tuning of the Band Gap and Redox Potential of Graphene Quantum Dots. *J. Phys. Chem. Lett.* **2011**, *2*, 1119–1124.
14. Mueller, M. L.; Yan, X.; McGuire, J. A.; Li, L.-s. Triplet States and Electronic Relaxation in Photoexcited Graphene Quantum Dots. *Nano Lett.* **2010**, *10*, 2679–2682.
15. Ji, Z.; Wu, R.; Adamska, L.; Velizhanin, A. K.; Doorn, S. K.; Sykora, M. *In Situ* Synthesis of Graphene Molecules on TiO_2. Application in Sensitized Solar Cells. *ACS Appl. Mater. Interfaces* **2014**, *6*, 20473–20478.
16. Cataldo, F.; Iglesias-Groth, S.; Manchado, A. Electronic Absorption Spectroscopy of Polycyclic Aromatic Hydrocarbons (PAHs) Radical Cations Generated in Oleum: A Superacid Medium. *Spectrochim. Acta Mol. Biomol. Spectrosc.* **2010**, *77*, 998–1004.
17. Khan, Z. H.; Husain, M. M.; Haselbach, E. On the Correlation between Electronic Spectra of Alternative Aromatic Hydrocarbons and Their Radical Cations. *Appl. Spectrosc.* **1993**, *47*, 2140–2144.
18. Dominikowska, J.; Domagala, M.; Palusiak, M. UV-Vis Spectra of Singlet State Cationic Polycyclic Aromatic Hydrocarbons: Time-dependent Density Functional Theory Study. *J. Chem. Phys.* **2014**, *140*, 044324.
19. Einholz, R.; Bettinger, H. F. Heptacene: Increased Persistence of a 4n+2 π-Electron Polycyclic Aromatic Hydrocarbon by Oxidation to the 4n π-Electron Dication. *Angew. Chem., Int. Ed.* **2013**, *52*, 9818–9820.
20. Ekiz, O. Ö.; Urel, M.; Güner, H.; Mizrak, A. K.; Dâna, A. Reversible Electrical Reduction and Oxidation of Graphene Oxide. *ACS Nano* **2011**, *5*, 2475–2482.
21. Polat, E. O.; Kocabas, C. Broadband Optical Modulators Based on Graphene Supercapacitors. *Nano Lett.* **2013**, *13*, 5851–5857.
22. Kristensen, E. W.; Igo, D. H.; Elder, R. C.; Heineman, W. R. Non-ideal Behavior of Nernstian Plots from Spectroelectrochemistry Experiments. *J. Electroanal. Chem.* **1991**, *309*, 61–72.
23. Bisquert, J.; Garcia-Belmonte, G.; Garcia-Canadas, J. Effects of Gaussian Energy Dispersion on the Statistics of Polarons and Bipolarons in Conducting Polymers. *J. Chem. Phys.* **2004**, *120*, 6726–6733.

24. Ardo, S.; Achey, D.; Morris, A. J.; Abrahmsson, M.; Meyer, G. J. Non-Nernstian Two-Electron Transfer Photocatalysis at Metalloporphyrin TiO_2 Interfaces. *J. Am. Chem. Soc.* **2011**, *133*, 16572–16580.
25. Mortimer, R. J. Electrochromic Materials. *Annu. Rev. Mater. Res.* **2011**, *41*, 241–268.
26. Monk, P. M. S.; Mortimer, R. J.; Rosseinsky, D. R. *Electrochromism*; Cambridge University Press: New York, 2007.
27. Polat, E. O.; Balci, O.; Kocabas, C. Graphene Based Flexible Electrochromic Devices. *Sci. Rep.* **2014**, *4*, No. 6484.
28. Kurum, U.; Ekiz, O. O.; Yaglioglu, H. G.; Elmali, A.; Urel, M.; Guner, H. X.; Zrak, A. K.; Ortac, B.; Dana, A. Electrochemically Tunable Ultrafast Optical Response of Graphene Oxide. *Appl. Phys. Lett.* **2011**, *98*, 141103.
29. Runnerstrom, E. L.; Llordes, A.; Lounis, S. D.; Milliron, D. J. Nanostructured Electrochromic Smart Windows: Traditional Materials and NIR-Selective Plasmonic Nanocrystals. *Chem. Commun.* **2014**, *50*, 10555–10572.
30. Dyer, A. L.; Craig, M. R.; Babiarz, J. E.; Kiyak, K.; Reynolds, J. R. Orange and Red to Transmissive Electrochromic Polymers Based on Electron-rich dDioxythiophenes. *Macromolecules* **2010**, *43*, 4460–4467.
31. Hoertz, P. G.; Chen, Z.; Kent, C. A.; Meyer, T. J. Application of High Surface Area Tin-Doped Indium Oxide Nanoparticle Films as Transparent Conducting Electrodes. *Inorg. Chem.* **2010**, *49*, 8179–8181.
32. Lyons, M. E. G.; Fray, H. G.; McCabe, T.; Corish, J. Charge Percolation in Electroactive Polymer Films. *J. Chem. Soc., Faraday Trans.* **1990**, *86*, 2905–2910.
33. Birks, J. B. *Photophysics of Aromatic Molecules*; Wiley-Interscience: London, 1970.